Iron Imido Complexes

DOI: 10.1002/ange.200602799

A Tosylimido Analogue of a Nonheme Oxoiron(IV) Complex**

Eric J. Klinker, Timothy A. Jackson, Michael P. Jensen, Audria Stubna, Gergely Juhász, Emile L. Bominaar, Eckard Münck, and Lawrence Que, Jr.**

High-valent nonheme iron complexes play key roles as intermediates in biology and catalysis.[1–3] Examples of oxoiron(IV) centers in nonheme ligand environments have been characterized in both enzymes[4,5] and model systems[6] and have been shown to participate in the hydroxylation of C–H bonds.[7,8] The analogous imidoiron(IV) unit should be capable of isolobal amination reactions and has been implicated in such iron-catalyzed reactions;[9] it is also proposed to be an intermediate in the formation of an isolated amidoiron(III) complex.[10] The only two structurally characterized examples of an imidoiron(IV) unit show this group in a tetrahedral geometry supported by a tridentate pyrazolyl/bis(phosphino)borate ligand[11] or as part of a novel $\{Fe^{III}{}_3Fe^{IV}(NR)_4\}$ cubane cluster.[12] In this paper, we report the generation and characterization of the tosylimidoiron(IV) analogue of the well-characterized oxoiron(IV) complex $[Fe^{IV}(O)(N4Py)]^{2+}$ (N4Py = *N*,*N*-bis(2-pyridylmethyl)bis(2-pyridyl)methylamine).[13] This first example of a pair of complexes with a ligand that can support both an oxo- and imidoiron(IV) unit provides a unique opportunity for a comparative study.

[*] Dr. A. Stubna, Dr. G. Juhász, Prof. Dr. E. L. Bominaar, Prof. Dr. E. Münck
Department of Chemistry
Carnegie Mellon University
Pittsburgh, PA 15213 (USA)
Fax: (+1) 412-268-1061
E-mail: emunck@cmu.edu
E. J. Klinker, Dr. T. A. Jackson, Dr. M. P. Jensen, Prof. Dr. L. Que, Jr.
Department of Chemistry and
Center for Metals in Biocatalysis
University of Minnesota
Minneapolis, MN 55455 (USA)
Fax: (+1) 612-624-7029
E-mail: que@chem.umn.edu

[**] Supported by NIH grants GM-33162 (L.Q.) and GM-22701 (E.M.), an NIH postdoctoral fellowship to T.A.J., and an NSF graduate research fellowship to A.S. XAS data were collected at the Stanford Synchrotron Radiation Laboratory (SSRL), which is supported by the US Department of Energy and the National Institutes of Health.

Supporting information for this article is available on the WWW under http://www.angewandte.org or from the author.

The oxoiron(IV) complex $[Fe^{IV}(O)(N4Py)]^{2+}$ (**1**) can be readily generated in high yield by oxygen-atom transfer from solid iodosylbenzene (PhIO) to $[Fe^{II}(NCMe)(N4Py)]^{2+}$ in MeCN.[8] In an analogous manner, the tosylimidoiron(IV) complex $[Fe^{IV}(NTs)(N4Py)]^{2+}$ (**2**) was prepared by treating the iron(II) precursor in MeCN with solid mesityl-*N*-tosylimidoiodinane (MsINTs; Ms = 2,4,6-$Me_3C_6H_2$, Ts = tosyl) at room temperature. Within minutes of the addition, the orange solution of the iron(II) starting material faded to a gold color. Complex **2** exhibits a visible spectrum (Figure 1) with an intense band at $\lambda = 445$ nm ($\varepsilon = 2700\,M^{-1}cm^{-1}$) and a much weaker and broader feature at $\lambda = 660$ nm ($\varepsilon = 250\,M^{-1}cm^{-1}$, Figure 1 inset). The latter may correspond to the band at $\lambda =$ 695 nm ($\varepsilon = 400\,M^{-1}cm^{-1}$, Figure 1 inset) observed for **1** that arises from ligand-field transitions characteristic of an $S = 1$ oxoiron(IV) center.[14] Complex **2** has a Mössbauer spectrum at 4.2 K that consists of a doublet with a quadrupole splitting of 0.93 mm s^{-1} and an isomer shift of 0.02 mm s^{-1}, parameters that fall within the range of those found for nonheme oxoiron(IV) complexes.[2] It gives rise to a high-resolution electrospray mass spectrum with a major ion species at *m*/*z* 741.0860 that corresponds to $[\{Fe^{IV}(NTs)(N4Py)\}(SO_3CF_3)]^+$ (*m*/*z* calculated 741.0859).

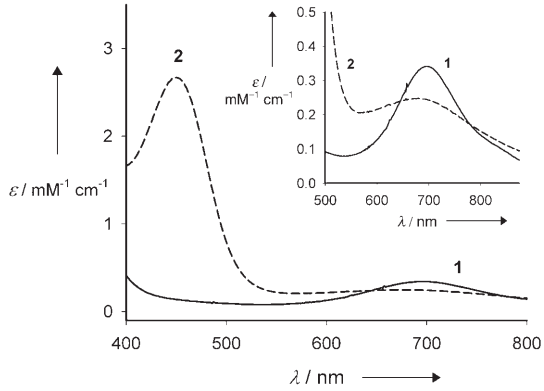

Figure 1. Visible spectra of $[Fe^{IV}(X)(N4Py)]^{2+}$ in MeCN (X = O, **1**; X = NTs, **2**). Inset: Vertically expanded lower-energy region.

The ^{1}H NMR spectrum of **2** (Figure 2) is similar to, but distinct from, that of **1**. Like **1**, complex **2** exhibits two equally intense sets of paramagnetically shifted pyridine ring protons, indicating the presence of an effective mirror plane of symmetry on the NMR time scale. The pyridine protons display a unique shift pattern arising from the $S = 1$ iron(IV) center[13] in which one pyridine β-proton signal is downfield-shifted to about $\delta = 45$ ppm, the other β-proton signal is upfield-shifted to about $\delta = -15$ ppm, and the γ-proton peak is downfield-shifted to about $\delta = 18$ ppm. The ^{1}H NMR spectrum of **2** also shows the presence of a small amount of **1**; the latter arises from trace water in the solvent that

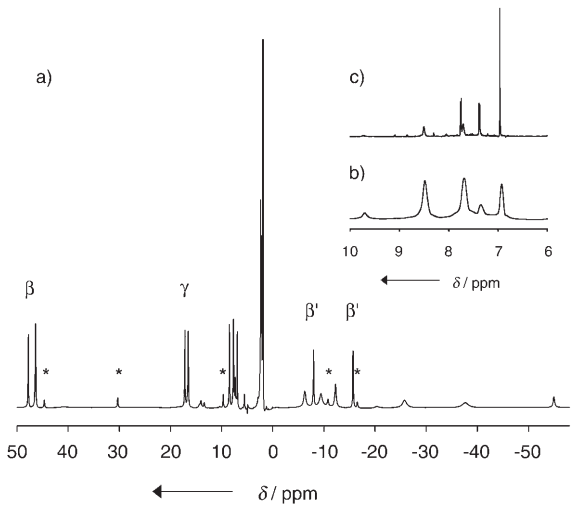

Figure 2. ^{1}H NMR spectrum of **2** in CD_3CN. Peaks assigned to a minor impurity of **1** are marked by (*). Insets show the $\delta = 6$–10 ppm region for **2** under conditions to enhance paramagnetically shifted protons (b) and under normal ^{1}H NMR conditions (c).

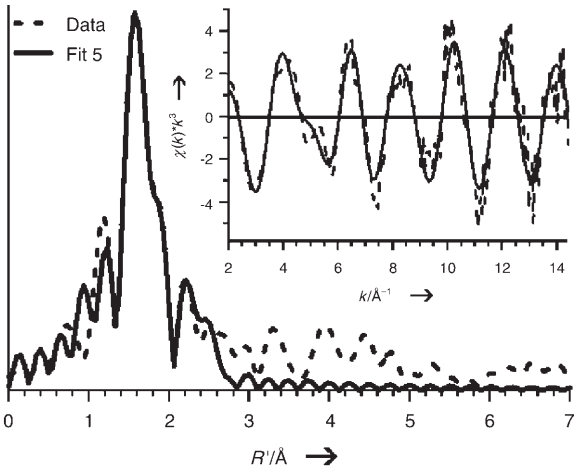

Figure 3. Fourier transform of the Fe K-edge EXAFS data and EXAFS spectrum (inset) of $[Fe^{IV}(NTs)(N4Py)]^{2+}$. Experimental data are shown in dashed lines and fits in solid lines. See the Supporting Information for EXAFS and Fourier transform range.

hydrolyzes part of the MsINTs oxidant to MsIO (**2** is not converted into **1** by the addition of trace water). The tosyl aromatic protons are observed at $\delta = 8.50$ and 7.71 ppm (Figure 2b), with integrations that match the values found for the pyridine proton peaks of **2**. With ^{1}H NMR parameters used for diamagnetic compounds, these tosyl resonances become obscured by peaks at $\delta = 7.75$ and 7.37 ppm (Figure 2c) corresponding to the protons of free tosylamide. The integrations of these peaks relative to that of the aromatic protons of the iodomesitylene by-product ($\delta = 6.95$ ppm) reveal an amount of free tosylamide (20%) that corresponds well to the amount of **1** present in the sample (15%). These data further support the formulation of **2** as $[Fe^{IV}(NTs)(N4Py)]^{2+}$.

Fe K-edge X-ray absorption spectroscopy (XAS) provides additional insight into the geometric and electronic structure of **2**. Complexes **1** and **2** exhibit 1s→3d transitions at about 7114 eV with areas of 25 and 18 units, respectively (Supporting Information).[15] As discussed previously, the relatively large value observed for **1** is a result of the short Fe–O bond length of 1.64 Å;[15] consequently, the pre-edge area of 18 suggests a smaller degree of distortion for the iron center of **2**, namely, a relatively long Fe–NTs bond. Indeed, a similar value was recently observed for the thiolate-ligated oxo-iron(IV) complex $[Fe^{IV}(O)(tmcs)]^+$ (tmcs = monoanion of 1-mercaptoethyl-4,8,11-trimethyl-1,4,8,11-tetraazacyclotetradecane), which, on the basis of an EXAFS analysis, exhibits a somewhat longer Fe–O bond (1.70 Å).[16]

An analysis of the EXAFS data obtained for **2** provides metric details of the iron coordination environment. In Figure 3 are displayed the *R*′-space and *k*-space EXAFS spectra of **2** along with the best fit to these data (see the Supporting Information for fitting details). The EXAFS data for **2** are well fit with three shells consisting of one N scatterer at 1.73 Å, five N scatterers at 1.97 Å, and six C scatterers at 2.87 Å. The latter two shells can be associated respectively with N and C atoms of the N4Py ligand, as observed in the X-ray crystal structure of **1**. The single scatterer at 1.73 Å is thus attributed to the N atom of the NTs ligand.

Notably, the Fe–N bond length found for **2** (1.73 Å) is significantly longer than the bond lengths observed crystallographically for the Fe–O bond in **1**[13] and for the Fe–N bonds of two other iron(IV) imido complexes (ca. 1.65 Å).[11,12] Relative to the latter two complexes, the longer bond in **2** can be rationalized by the difference in the coordination numbers of the iron(IV) centers. The previously characterized complexes have a tetrahedral geometry about the iron center with a strong trigonal distortion for which the π-antibonding molecular orbitals (MOs) associated with the imido ligand are unoccupied.[3] These complexes thus have a formal Fe≡NR triple bond and a collinear Fe-N-R unit.[3,11,12] In contrast, the corresponding MOs for octahedral **2** are singly occupied, thus giving rise to an Fe=N double bond instead. This experimental result is supported by a DFT geometry-optimized structure for **2** (Figure 4a and the Supporting Information), which is constrained to have C_s symmetry to be consistent with the NMR results and displays a Fe–NTs bond length of 1.75 Å.

The effects of the different Fe=X units in **1** and **2** on their ground-state electronic structures were revealed by high-field Mössbauer analysis; the experimental results were complemented by DFT calculations that were based on the geometry-optimized structures for **1** and **2** (see the Supporting Information). Variable-temperature Mössbauer spectra for **1** and **2** in acetonitrile were obtained in applied magnetic fields of up to 8.0 T; spectra of each compound at 4.2 K are shown in Figure 5. The spectra were simulated by using the $S = 1$ spin Hamiltonian of Equation (1), in which all symbols have their conventional meanings.[17]

$$H = D(S_z^2 - {}^2/_3) + E(S_x^2 - S_y^2) + \beta \mathbf{B}\,\mathbf{g}\,\mathbf{S} + \mathbf{S}\,\mathbf{A}\,\mathbf{I} - g_n\beta_n\,\mathbf{I}\,\mathbf{B} + H_Q$$
$$H_Q = \frac{e\,Q\,V_{zz}}{12}\left[3\,I_z^2 - \frac{15}{4} + \eta(I_x^2 - I_y^2)\right] \quad (1)$$

Analysis of the spectra of **1** shows that the magnetic hyperfine tensor, **A**, and the zero-field splitting (ZFS) tensor

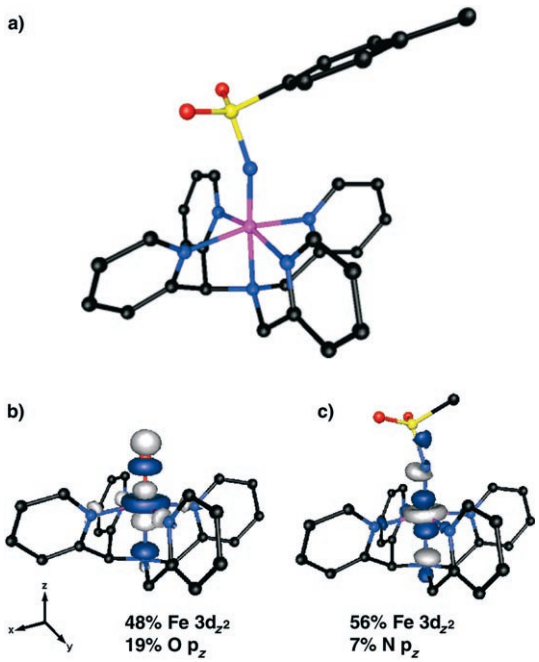

Figure 4. Molecular structure of $[Fe^{IV}(NTs)(N4Py)]^{2+}$ based on DFT geometry optimization (a), and contour plots of the Fe $3d_{z^2}$-based MOs of $[Fe^{IV}(O)(N4Py)]^{2+}$ (b) and $[Fe^{IV}(NTs)(N4Py)]^{2+}$ (c) based on DFT computations. Fe purple, C black, N blue, O red, S yellow. The contributions to the MOs from the Fe $3d_{z^2}$ and oxo O and imido N 2p orbitals are displayed. For clarity in (c), the tolyl ring is not shown.

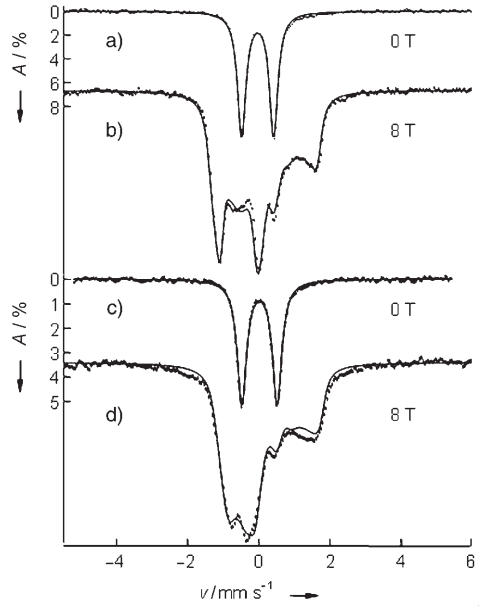

Figure 5. Mössbauer spectra of **1** (a, b) and **2** (c, d) in CH_3CN at 4.2 K. Spectra in (a) and (c) were obtained in zero field while those in (b) and (d) were obtained in a magnetic field of 8.0 T applied parallel to the observed γ rays. The solid lines are spectral simulations based on the $S=1$ Hamiltonian of Equation (1) using the parameters in Table 1 and in Table S2 of the Supporting Information. Both **1** and **2** contained minor contaminants; for clarity, their contributions were removed from the spectra. A complete set of data, spectral simulations, and information about the contaminants are given in the Supporting Information.

are both axial (that is, $A_x = A_y$ and $E/D = 0$) and that A_z lies along the symmetry axis of the ZFS tensor (Table 1). DFT computations for **1** also yield an axial **A** tensor, with A_z aligned within 10° of the Fe–O bond. Our combined DFT/crystal-field studies of previous complexes[14,16,18] and **1** suggest that the z axis of the ZFS tensor and therefore of Equation (1) is along the Fe–O vector.

Table 1: Properties of $[Fe^{IV}(NTs)(N4Py)]^{2+}$ (**2**) and $[Fe^{IV}(O)(N4Py)]^{2+}$ (**1**) complexes.[a]

	$[Fe^{IV}(NTs)(N4Py)]^{2+}$	$[Fe^{IV}(O)(N4Py)]^{2+}$
$t_{1/2}$ at 25 °C [h]	3 h	60 h
r(Fe–N/O) [Å]	1.73 (1.75)	1.64[b] (1.65)
	1.97 (2.01)	1.96 (2.01)
λ_{max} [nm] {ε [$M^{-1}cm^{-1}$]}	445 {2700}	
	660 {250}	695 {400}
δ [mm s^{-1}]	0.02 (0.13[c])	−0.04 (0.03[c])
ΔE_Q [mm s^{-1}]	+0.98 (1.13)	+0.93 (1.03)
η	−0.7 (−1.2)	$0<\eta<0.5$ (0.01)
D [cm^{-1}]	29	22
E/D	0.23	0
$A_x/g_n\beta$ [T][d,e]	−20 (−20.5)	−21 (−20.3)
$A_y/g_n\beta_n$ [T][d,e]	−21 (−18.3)	−21 (−20.8)
$A_z/g_n\beta_n$ [T][d,e]	−3 (−5)	−5 (−4.1)
E_o [eV]	7123.8	7123.7[f]
$E_{pre\text{-}edge}$ [eV]	7113.9	7114.3[f]
pre-edge area	18	25[f]

[a] Values in parentheses derived from DFT calculations (see the Supporting Information for details). [b] Obtained by X-ray crystallography; see reference [13]. [c] For the N4Py ligand, for reasons not yet understood, our computations yield δ values noticeably larger than those observed experimentally. Rotation of the tosyl group around the Fe–N bond, followed by geometry optimization, changed the δ value by less than 0.02 mm s^{-1}. [d] Final A values were obtained by adding the calculated spin–dipolar contribution to the experimental value $A_{iso} = (A_x + A_y + A_z)/3$. We used this procedure because DFT A_{iso} values generally are in poor agreement with experimental data. The z axes of the electric-field gradient tensor and the spin–dipolar part of **A** are coincident within 5° with the Fe–NTs bond axis. [e] At 4.2 K the internal field $B_{int} \approx \{g_\perp A_\perp S(S+1)/D\}\beta B/g_n\beta_n$ and thus the product $g_\perp A_\perp$, rather than $A_\perp$, is determined, thereby illustrating the point for axial symmetry. In our simulations we have fixed $g_\perp = 2$. The real $A_\perp$ value may be slightly smaller but probably not by more than 10%. As an example, the correction is about 1% for $[Fe^{IV}(O)(tmcs)]^+$ as calculated by time-dependent DFT.[16] [f] From reference [15].

The applied-field Mössbauer spectra of **2** are quite distinct from those of **1** (Figure 5b,d). These differences arise from a substantial anisotropy of the magnetic hyperfine field ($\mathbf{B}_{int} = -\langle \mathbf{S} \rangle \mathbf{A}/g_n\beta_n$) in the xy plane of **2** (for example, 3.3 T in the spectrum of Figure 5d). This anisotropy can be caused by a rhombic ZFS tensor ($E/D \neq 0$) and/or by a rhombic **A** tensor ($A_x \neq A_y$). Although the Mössbauer data do not allow us to determine these three parameters independently, the expression $A_\perp = (A_x + A_y)/2$ is nearly independent of the E/D value used to fit the spectra. For C_s symmetry, implied by the ^{1}H NMR spectrum of **2** (Figure 2), the anisotropy of **A** is determined by the spin–dipolar contribution, $\mathbf{A}_{S\text{-}D}$. As DFT calculations on **2** yield a nearly axial $\mathbf{A}_{S\text{-}D}$, ($A_{jj}/g_n\beta_n = -3.5, -5, +8.5$ T for $j = x$, y, and z, respectively), we conclude that the magnetic anisotropy of **2** is a result of a finite E/D value of

0.23, determined by fitting the Mössbauer spectra of **2** with a nearly axial **A** tensor. For **2** we found that $A_\perp/g_n\beta_n$ is about −20.5 T if $S=1$ is assumed, a value which fits well in the range −20 T to −23 T observed for $S=1$ complexes.[6,16,19] In contrast, fitting the spectra of **2** under assumption of an $S=2$ ground state yielded $A_\perp/g_n\beta_n \approx -6.5$ T, which, in magnitude, is substantially below $-A_\perp/g_n\beta_n = 16$–20 T observed for $S=2$ Fe^{IV} species.[4,20]

Nonheme oxoiron(IV) complexes exhibit large D values, which arise from spin–orbit coupling of the $S=1$ ground state with low-lying $S=2$ excited states.[16,18] Importantly, this coupling modifies the D value but affects the **g** and **A** tensors of Equation (1) in a minor way at most. Spin–orbit coupling with low-lying $S=1$ excited states would give rise to substantially smaller $A_\perp/g_n\beta_n$ values owing to partial unquenching of the orbital angular momentum and give a positive contribution to **A**.[21] Because this is not the case for **1** and **2**, we conclude that spin–orbit coupling of the ground state with low-lying $S=2$ and/or $S=0$ excited states is responsible for the large D value, as shown in the Supporting Information.

The DFT calculations also shed light on the dominant bonding interactions that determine the differing Fe=X bond lengths of **1** and **2**. For both systems, a $(3d_{xy})^2(3d_{xz})^1(3d_{yz})^1$ electronic configuration is observed, thus consistent with formal Fe=O and Fe=NR bonds. As evidenced by the almost equal mixture of Fe 3d and oxo O 2p or imido N 2p character in the Fe $3d_{xz}$- and $3d_{yz}$-based MOs, both complexes exhibit strong Fe=X π bonds. However, differences between **1** and **2** are apparent in the Fe $3d_{z^2}$-based MOs. For **1**, a strong σ-antibonding interaction between the $3d_{z^2}$ orbital and the O p_z orbital (Figure 4a) splits the spin-up Fe $3d_{x^2-y^2}$- and $3d_{z^2}$-based MOs by roughly 0.6 eV (Supporting Information). In contrast, the corresponding MOs of **2** are nearly degenerate (split by only about 0.05 eV). This is a result of a less favorable interaction between the Fe $3d_{z^2}$ and the N p_z-like orbital of the tosylimido ligand (Figure 4c), the latter of which is stabilized relative to the corresponding N $2p_y$ and $2p_x$ orbitals owing to the N–S bonding interaction. Thus, these DFT studies reveal that, despite the fact that both **2** and **1** contain formal Fe=N and Fe=O bonds, respectively, the Fe–O σ interaction of **1** is significantly stronger than the corresponding Fe–NTs interaction in **2**, which accounts in part for the relatively long Fe–NTs bond length of 1.73 Å.

The longer Fe–N bond of **2** suggests that the tosylimido group may not be able to stabilize the iron(IV) center as well as the oxo ligand in **1**. Indeed, **2** has a half-life of three hours for self-decay at room temperature, which is a factor of 20 shorter than that of **1**. This difference is also consistent with the faster transfer of NTs from PhINTs (versus PhIO) to the pendant phenyl group of $[Fe^{II}(6\text{-Ph-tpa})]^{2+}$ (tpa = tris(2-pyridylmethyl)amine).[9a] Further studies are clearly warranted to understand the relative oxidative abilities of Fe^{IV}=O and Fe^{IV}=NR units and to place them within the greater context of recently reported high-valent nitridoiron complexes.[22]

Received: July 13, 2006
Published online: October 13, 2006

Keywords: bioinorganic chemistry · density functional calculations · imido ligands · iron · Mössbauer spectroscopy

[1] M. Costas, M. P. Mehn, M. P. Jensen, L. Que, Jr., *Chem. Rev.* **2004**, *104*, 939.
[2] X. Shan, L. Que, Jr., *J. Inorg. Biochem.* **2006**, *100*, 421.
[3] M. P. Mehn, J. C. Peters, *J. Inorg. Biochem.* **2006**, *100*, 634.
[4] J. C. Price, E. W. Barr, B. Tirupati, J. M. Bollinger, Jr., C. Krebs, *Biochemistry* **2003**, *42*, 7497.
[5] D. A. Proshlyakov, T. F. Henshaw, G. R. Monterosso, M. J. Ryle, R. P. Hausinger, *J. Am. Chem. Soc.* **2004**, *126*, 1022; P. J. Riggs-Gelasco, J. C. Price, R. B. Guyer, J. H. Brehm, E. W. Barr, J. M. Bollinger, Jr., C. Krebs, *J. Am. Chem. Soc.* **2004**, *126*, 8108.
[6] J.-U. Rohde, J.-H. In, M.-H. Lim, W. W. Brennessel, M. R. Bukowski, A. Stubna, E. Münck, W. Nam, L. Que, Jr., *Science* **2003**, *229*, 1037; M. H. Lim, J.-U. Rohde, A. Stubna, M. R. Bukowski, M. Costas, R. Y. N. Ho, E. Münck, W. Nam, L. Que, Jr., *Proc. Natl. Acad. Sci. USA* **2003**, *100*, 3665.
[7] J. C. Price, E. W. Barr, T. E. Glass, C. Krebs, J. M. Bollinger, Jr., *J. Am. Chem. Soc.* **2003**, *125*, 13008.
[8] J. Kaizer, E. J. Klinker, N. Y. Oh, J.-U. Rohde, W. J. Song, A. Stubna, J. Kim, E. Münck, W. Nam, L. Que, Jr., *J. Am. Chem. Soc.* **2004**, *126*, 472.
[9] M. P. Jensen, M. P. Mehn, L. Que, Jr., *Angew. Chem.* **2003**, *115*, 3940; *Angew. Chem. Int. Ed.* **2003**, *42*, 4357; F. Avenier, J.-M. Latour, *Chem. Commun.* **2004**, 1544.
[10] R. L. Lucas, D. R. Powell, A. S. Borovik, *J. Am. Chem. Soc.* **2005**, *127*, 11596.
[11] C. M. Thomas, N. P. Mankad, J. C. Peters, *J. Am. Chem. Soc.* **2006**, *128*, 4956.
[12] A. K. Verma, T. N. Nazif, C. Achim, S. C. Lee, *J. Am. Chem. Soc.* **2000**, *122*, 11013.
[13] E. J. Klinker, J. Kaizer, W. W. Brennessel, N. L. Woodrum, C. J. Cramer, L. Que, Jr., *Angew. Chem.* **2005**, *117*, 3756; *Angew. Chem. Int. Ed.* **2005**, *44*, 3690.
[14] A. Decker, J.-U. Rohde, L. Que, Jr., E. I. Solomon, *J. Am. Chem. Soc.* **2004**, *126*, 5378.
[15] J.-U. Rohde, S. Torelli, X. Shan, M. H. Lim, E. J. Klinker, J. Kaizer, K. Chen, W. Nam, L. Que, Jr., *J. Am. Chem. Soc.* **2004**, *126*, 16750.
[16] M. R. Bukowski, K. D. Koehntop, A. Stubna, E. L. Bominaar, J. A. Halfen, E. Münck, W. Nam, L. Que, Jr., *Science* **2005**, *310*, 1000.
[17] E. Münck in *Physical Methods in Bioinorganic Chemistry. Spectroscopy and Magnetism* (Ed.: L. Que, Jr.), University Science Books, Sausalito, CA, **2000**, p. 287.
[18] J. C. Schoneboom, F. Neese, W. Thiel, *J. Am. Chem. Soc.* **2005**, *127*, 5840.
[19] C. V. Sastri, M. J. Park, T. Ohta, T. A. Jackson, A. Stubna, M. S. Seo, J. Lee, J. Kim, T. Kitagawa, E. Münck, L. Que, Jr., W. Nam, *J. Am. Chem. Soc.* **2005**, *127*, 12494; J. Bautz, M. R. Bukowski, M. Kerscher, A. Stubna, P. Comba, A. Lienke, E. Münck, L. Que, Jr., *Angew. Chem.* **2006**, *118*, 5810; *Angew. Chem. Int. Ed.* **2006**, *45*, 5681.
[20] K. L. Kostka, B. G. Fox, M. P. Hendrich, T. J. Collins, C. E. F. Richard, L. J. Wright, E. Münck, *J. Am. Chem. Soc.* **1993**, *115*, 6746; O. Pestovsky, S. Stoian, E. Bominaar, X. Shan, E. Münck, L. Que, Jr., A. Bakac, *Angew. Chem.* **2005**, *117*, 7031; *Angew. Chem. Int. Ed.* **2005**, *44*, 6871.
[21] W. T. Oosterhuis, G. Lang, *J. Chem. Phys.* **1973**, *58*, 4757.
[22] T. A. Betley, J. C. Peters, *J. Am. Chem. Soc.* **2004**, *126*, 6252; N. Aliaga-Alcalde, S. DeBeer George, B. Mienert, E. Bill, K. Wieghardt, F. Neese, *Angew. Chem.* **2005**, *117*, 2968; *Angew. Chem. Int. Ed.* **2005**, *44*, 2908; J. F. Berry, E. Bill, E. Bothe, S. D. George, B. Mienert, F. Neese, K. Wieghardt, *Science* **2006**, *312*, 1937.

